Empirical determination of the kaon distribution amplitude

Lei Chang,[1,*] Yu-Bin Liu,[1] Khépani Raya,[2,†] and M. Atif Sultan[1,3,‡]

[1]*School of Physics, Nankai University, Tianjin 300071, China*

[2]*Department of Integrated Sciences and Center for Advanced Studies in Physics, Mathematics and Computation, University of Huelva, E-21071 Huelva, Spain*

[3]*Centre For High Energy Physics, University of the Punjab, Lahore 54590, Pakistan*

(Received 10 April 2025; accepted 25 November 2025; published 31 December 2025)

We propose a data-driven approach to extract the kaon leading-twist distribution amplitude (DA) from empirical information on the ratio of the neutral-to-charged kaon electromagnetic form factors, $\mathcal{R}_K$. Our study employs a two-parameter representation of the DA at $\zeta = 2$ GeV, designed to capture the expected broadening and asymmetry of the distribution, as well as the soft endpoint behavior predicted by quantum chromodynamics (QCD). Our leading-order analysis of the latest experimental measurements of $\mathcal{R}_K$ reveals that the extracted DA exhibits a somewhat significant skewness, with the first symmetric moment being approximately $\langle 1-2x\rangle_K = 0.082(7)$. On the other hand, the broadness and general shape of the produced distributions show a reasonable consistency with contemporary lattice and continuum QCD analyses. These findings highlight the importance of accurately determining the profile of the DA, especially the skewness and its relation to $SU_F(3)$ flavor symmetry breaking, as well as the inclusion of higher-order effects in the hard-scattering kernels for analyzing data at experimentally accessible scales.

DOI: 10.1103/3hd9-7wnt

I. INTRODUCTION

The BESIII experiment has recently achieved a groundbreaking measurement of the ratio of neutral-to-charged kaon electromagnetic form factors (EMFFs) in the large-momentum-transfer regime ($12 < Q^2 < 25$ GeV^2) [1]. A constant value for this ratio, 0.21 ± 0.01, was determined. Its small yet notable size exposes the $SU_F(3)$ flavor symmetry breaking (FSB) in the kaon wave function. Notably, the BESIII result aligns with a previous measurement at $|Q^2| = 17.4$ GeV^2 [2]. This exploration identifies an apparent discrepancy between the empirical extractions of the ratio of charged pion-to-kaon EMFFs and the predictions from quantum chromodynamics (QCD) at leading-order (LO) in perturbation theory [3–6], where the so-called distribution amplitude (DA) plays a pivotal role. The results of [2] are also seemingly inconsistent with projections based on nonperturbative frameworks [7]. On its part, the recent analysis from Ref. [8] derives next-to-next-to-leading order (NNLO) corrections to the LO hard-scattering formulas (HSF) from Refs. [3–5], expanding the next-to-leading order (NLO) results from Refs. [9–12]. Subsequently, employing recent lattice QCD (lQCD) determinations for the leading-twist kaon DA [13], the exploration from Ref. [14] underscores the significant impact of higher-order contributions on the large-Q^2 regime of the EMFFs. Higher-order and higher-twist effects have been explored in both collinear and k_T factorization [15,16]. These observations are reinforced by the lQCD computation of the pion and kaon EMFFs at large momenta [17]. Current and planned experimental efforts will certainly provide valuable insights on these aspects [18,19].

For the above, the importance of accurately determining the kaon DA is clear, but this need extends further. Kaons and pions are the Nambu-Goldstone bosons of dynamical chiral symmetry breaking (DCSB), so their existence and properties are deeply connected to the mass generation mechanisms in the Standard Model [20–22]. In the absence of Higgs fields (HF), these states would be massless and identical. The structural differences observed in real life arise from the $SU_F(3)$ FSB, whose size is controlled by the interplay between the HF and QCD's mass generation. The shape of the DA is highly sensitive to this confluence: its broadness reflects the effects of DCSB, while its skewness would be influenced by both DCSB and the magnitude of FSB [22]. Several studies have demonstrated that the pion

*Contact author: leichang@nankai.edu.cn

†Contact author: khepani.raya@dci.uhu.es

‡Contact author: atifsultan.chep@pu.edu.pk

DA is broader than its asymptotic form at experimentally accessible energy scales (e.g., Refs. [13,23–32]). In contrast, lQCD and continuum analyses reveal that the heavy-quarkonia distributions are markedly narrower [33–36]. This reflects the fact that DCSB becomes less relevant as the current quark masses increase. In fact, heavy quarkonia systems approach a nonrelativistic limit in which both quarks carry a momentum fraction $x \approx 1/2$, resulting in a strong endpoint suppression for the DA [37]. Regarding the kaon, continuum Schwinger methods (CSMs) [24,38], holographic models [28,29], lQCD and QCD sum rules [13,30,31,39], among others, all concur that its DA remains broad, though somewhat narrower than the pion's. Nonetheless, the degree of asymmetry is much less determined.

While the pion DA has been extensively studied using experimental data, particularly from elastic and two-photon transition form factors (e.g., Refs. [32,40,41]), it appears that no comparable analysis exists for the kaon. To address this gap, we propose an exploratory data-driven analysis for extracting the DA, which relies on leading-order HSF in QCD and the most recent experimental data on the neutral-to-charged kaon EMFFs [1]. This simplified LO approach permits

(i) Extracting the kaon DA empirically, ultimately leading to a data-driven constraint on the flavor asymmetry within the kaon wave function.
(ii) Evaluating the impact of skewness on the DA to determine how much this asymmetry alone can account for the measurements of the kaon EMFFs in the large-momentum transfer regime.
(iii) Assessing the validity of the current approach by comparing the resulting DAs with those from well-established frameworks.
(iv) Establishing the foundation for incorporating higher-order corrections. By first analyzing the role of the skewness in the DA at LO, we can better isolate and interpret the effects of higher-order corrections in future studies, enabling a more systematic exploration of the kaon structure.

The approach to be outlined not only addresses the key uncertainty in the pointwise behavior of the kaon DA but also provides a clear pathway for reconciling theoretical predictions with experimental data. In the end, our work aims to advance the understanding of the kaon's internal structure, with a particular focus on the role of $SU_F(3)$ FSB in dictating its properties.

The manuscript is organized as follows. We begin with the ratio of neutral-to-charged kaon form factors and its connection to the DAs through HSFs. Next, we present the data-driven construction of the DA at the starting scale 2 GeV. The resulting kaon EFFs are discussed in the following section. Finally, we summarize our findings and outline the scope of the present work.

II. RATIO OF NEUTRAL-TO-CHARGED KAON FORM FACTORS

Through HSFs in QCD, the EMFF of a pseudoscalar meson **P** can be expressed as a combination of hard and soft components. The former is, in principle, computable in perturbation theory; the soft part, on the other hand, encodes the nonperturbative effects via the DA [3–6].

At leading-order, the EMFF can be compactly expressed as follows:

$$Q^2 F_{\mathbf{P}}(Q^2) \overset{Q^2>Q_0^2}{\approx} 16\pi\alpha_s(Q^2) f_{\mathbf{P}}^2 \sum_f e_f w_f^2(Q^2), \tag{1}$$

where α_s is the one-loop strong running coupling and $f_{\mathbf{P}}$ the meson's leptonic decay constant ($f_K \approx 0.11$ GeV). The label f indicates the flavor of the valence-quark and e_f its electric charge in terms of that of the fundamental one. Note that the HSF hold at sufficiently high energies $Q_0^2 \gg \Lambda_{\rm QCD}^2$, though the precise Q_0^2 value is not inherently determined from QCD principles. The weight-factor $w_f(Q^2)$ is linked to the soft part in the HSF. This is defined as follows:

$$w_f(Q^2) = \frac{1}{3}\int dx \frac{\varphi_{\mathbf{P}}^f(x;Q^2)}{1-x}. \tag{2}$$

Here, $\varphi_{\mathbf{P}}^f(x;Q^2)$ represents the meson's leading-twist DA. Intuitively, it describes the likelihood of finding a valence-quark f to carry a momentum fraction x of the meson's total momentum. The antiquark distribution is straightforwardly obtained by replacing $x \to 1-x$. Our choice of Q^2 as the defining scale of the DA indicates that this has also been adopted as the factorization scale in Eq. (1). Note also that the appearance of α_s and the DA in the HSF expose the scaling violations of QCD [22,42].

We assume isospin symmetry under which the up (u) and down (d) quarks are treated as identical except for their electric charges. For notational convenience, these quarks will be referred to as l-quarks. This symmetry allows us to express the ratio of the neutral-to-charged kaon form factor, $\mathcal{R}_K(Q^2)$, as

$$\mathcal{R}_K(Q^2) := \frac{|F_{K^0}(Q^2)|}{|F_{K^+}(Q^2)|} \overset{Q^2>Q_0^2}{\approx} \left|\frac{-\frac{1}{3}w_l^2(Q^2)+\frac{1}{3}w_s^2(Q^2)}{\frac{2}{3}w_l^2(Q^2)+\frac{1}{3}w_s^2(Q^2)}\right|. \tag{3}$$

Such quantity provides a measure of the relative contributions of the valence-quarks to the kaon form factors, reflecting not only the interplay between the electric charges but also, through the corresponding DAs, the effects of FSB induced by the mass generation mechanisms.

The intuition above is further reinforced by considering the domain of asymptotically large energies ($Q^2 \to \infty$), where the DAs converge to [3–6]

$$\varphi^f_{\mathbf{P}}(x; Q^2 \to \infty) \to \varphi^{\text{asy}}(x) = 6x(1-x). \tag{4}$$

Within this region, the weight factors w_l and w_s approach unity [3,43], leading to a vanishing ratio $\mathcal{R}_K(Q^2 \to \infty) \to 0$. This would be the same case in the whole energy range, if w_l and w_s were identical. A nonzero value of $\mathcal{R}_K(Q^2)$ at finite values of Q^2 is therefore a reflection of the flavor asymmetry, measured through the asymmetry in the corresponding DAs. The skewness in the kaon DA encodes the differences in the momentum distributions of the l and s-quarks within the kaon, pointing out the role of flavor-dependent effects in the electromagnetic structure of mesons.

III. DISTRIBUTION AMPLITUDE AT 2 GEV

While various perspectives confirm certain features of the kaon DA, such as a broadness comparable to that of the pion (which itself is wider than the asymptotic profile $\varphi^{\text{asy}}(x)$ at accessible energies), the precise form of the kaon DA remains an open question. In particular, as previously noted, the extent of its asymmetry deserves special attention.

For the purpose of our discussion, we consider a leading-twist DA defined at a resolution scale $\zeta_2 = 2$ GeV, expressed via a two-parameter functional form as follows:

$$\varphi^l_{\mathbf{P}}(x;\zeta_2) = \mathcal{N}_{\mathbf{P}} \ln\left(1 + \frac{x(1-x)}{\rho^{\mathbf{P}}_0 + \rho^{\mathbf{P}}_1(2x-1)}\right). \tag{5}$$

Here, $\rho^{\mathbf{P}}_0$ and $\rho^{\mathbf{P}}_1$ are the parameters to be determined, and $\mathcal{N}^{\mathbf{P}}$ ensures the unit normalization of the DA. Adopting this representation has important advantages. First, the distribution's Mellin moments,

$$\langle (1-2x)^m \rangle^{\mathbf{P}}_{\zeta_2} = \int_0^1 dx\, \varphi^l_{\mathbf{P}}(x;\zeta_2)(1-2x)^m, \tag{6}$$

can be obtained algebraically. Second, despite the reduced number of parameters, the proposed form is capable of capturing the expected broadness and skewness of the light-meson DAs. For instance, the distributions reported in Ref. [24], obtained using sophisticated kernels (DB) within the CSMs framework, are accurately reproduced with

$$\rho^\pi_0 = 0.032, \quad \rho^\pi_1 = 0; \quad \rho^K_0 = 0.054, \quad \rho^K_1 = 0.013. \tag{7}$$

Meanwhile, the *rainbow-ladder* (RL) expectations from Refs. [23,38], are satisfied provided

$$\rho^\pi_0 = 0.003, \quad \rho^\pi_1 = 0; \quad \rho^K_0 = 0.133, \quad \rho^K_1 = 0.082. \tag{8}$$

Throughout the rest of the text, we will use these representations for the DB and RL expectations. Evidently, the asymmetry in $\varphi^l_{\mathbf{P}}(x;\zeta_2)$ arises from $\rho^{\mathbf{P}}_1$, whereas the broadness and all moments $\langle \xi^m \rangle^{\mathbf{P}}_{\zeta_2}$ are influenced by both $\rho^{\mathbf{P}}_0$ and $\rho^{\mathbf{P}}_1$. This contrasts with the logarithmic representation proposed in Ref. [22], where even moments are independent of the parameter controlling the skewness. We choose to keep this correlation between the model parameters. Finally, a desirable characteristic of Eq. (5) is that it faithfully captures the endpoint behavior prescribed by QCD, that is, $\varphi^l_{\mathbf{P}}(x \to 1) \sim (1-x)$.

These features make our parametrization more advantageous compared to alternative forms. For instance, approaches based on a $C_j^{3/2}$-Gegenbauer polynomial expansion may require a large number of terms to achieve the desired accuracy [23]. Alternatively, representations employing a multiplicative factor $x^\alpha(1-x)^\beta$ yield an incorrect endpoint behavior. This, in turn, results in a poor estimation of the $\langle x^{-1}, (1-x)^{-1} \rangle$ moments entering the HSF, preventing an accurate description of the large-Q^2 behavior of the EMFFs. By considering the form in Eq. (5), we aim to provide a more physically motivated yet flexible representation of the kaon DA, which maintains consistency with QCD predictions and existing phenomenological observations. Analogous forms have been successfully employed to determine distribution functions from a collection of Mellin moments [44].

In order to determine the model parameters that define $\varphi^l_K(x;\zeta_2)$, we adopt the following strategy:

(1) A random value $\rho^{(i)}_0$ is chosen from the interval (0,0.2).

(2) Given $\rho^{(i)}_0$, the parameter $\rho^{(i)}_1$ is randomly selected within a range that ensures

$$\langle \xi^2 \rangle^{(i)} \in (0.22, 0.26). \tag{9}$$

This constraint is informed by various continuum and lQCD studies [13,24,31,35,36,38].

(3) Once $\varphi^I_{(i)}$ is fully defined by the two parameters $\rho^{(i)}_{0,1}$, Eq. (3) is applied to compute $\mathcal{R}^{(i)}_K(Q^2)$ over a discrete set of Q^2_j values matching the experimental data points.

Note that for each Q^2_j, the DA is evolved from the starting scale $Q^2 = \zeta_2^2$ to Q^2_j, according to the LO evolution equations [4–6]. For this purpose, we set $\Lambda_{\text{QCD}} = 0.234$ GeV and $n_f = 4$ flavors.

(4) The resulting $\mathcal{R}^{(i)}_K(Q^2)$ is compared with the experimental data, where the error bars are symmetrized. If the computed $\chi^2/\text{d.o.f.} < 2$, the $\{\rho^{(i)}_0, \rho^{(i)}_1\}$ pair is retained.

(5) This process is repeated until 50 valid duplets are produced.

The outcome of this procedure is shown in Fig. 1. We observe that the generated set of DAs exhibits a notable agreement with the lQCD determination [13], though our results show a greater degree of asymmetry. Other

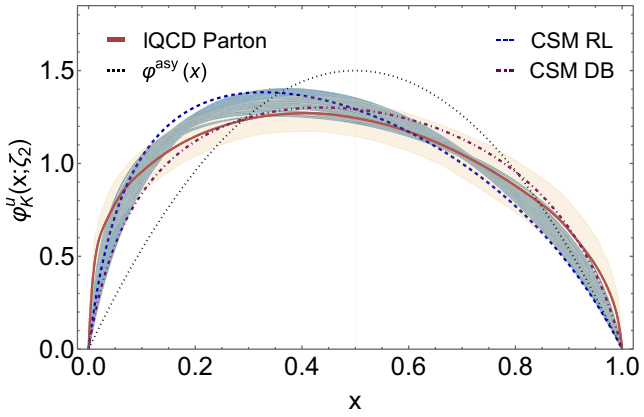

FIG. 1. Kaon leading-twist DAs at $\zeta = 2$ GeV, $\varphi_K^l(x;\zeta_2)$. Our set of replicas is drawn as light blue solid lines. For comparison, we include results from lQCD [13] and CSMs [24,38]. The black dotted curve represents the asymptotic profile $\varphi^{asy}(x) = 6x(1-x)$. Corresponding low-order Mellin moments are provided in Table I.

evaluations also fall within the ballpark, e.g., [28,29,31]. The same figure offers a comparison with the results from the CSMs, employing both RL and DB kernels [24,38]. The RL profile exhibits a more pronounced skewness, effectively setting a boundary. In contrast, the kaon DA derived from the DB kernel features a more symmetric shape. The peak of the DA provides a way to quantify its skewness. In our case, the distribution reaches its maximum at

$$x^{max} = 0.37(1), \tag{10}$$

reflecting a 25% deviation from the symmetric limit $x^{max} = 0.5$. The typical trend for this shift is around ∼20% [13,24,31,39]. Such a displacement is of the same order of the $f_K - f_\pi$ difference, quantities that serve as indicators of the strength of DCSB. This suggest that the skewness in the DA is primarily driven by QCD nonperturbative phenomena (mass generation) rather than the large disparity among the current-quark masses ($m_s/m_l \sim 20$) [20–22]. Notable exceptions to this pattern include the RL result, where the peak of the distribution is deviated around 33% from the symmetric case [38], and the lQCD analysis from [30], which, within uncertainties, yields a nearly symmetric kaon DA that resembles the asymptotic profile.

The evaluation carried out here leads to the following mean values:

$$\langle\xi\rangle_{\zeta_2}^K = 0.082(7), \qquad \langle\xi^2\rangle_{\zeta_2}^K = 0.239(9). \tag{11}$$

A comparison with the moments presented in Table I suggests that our prediction for $\langle\xi\rangle_{\zeta_2}^K$ exceeds the general trend, being surpassed only by the RL result. This quantity also encapsulates the degree of skewness and, consequently, the strength of the $SU_F(3)$ FSB. Unsurprisingly, the kaon DA's dilation (the effects of DCSB) are accurately captured, as demonstrated by the precise agreement of $\langle\xi^2\rangle_{\zeta_2}^K$ with phenomenological expectations.

TABLE I. Low-order Mellin moments of the kaon DA $\varphi_K^l(x;\zeta_2)$. The CSM DAs were expressed as in Eq. (5), employing the parameters from Eqs. (7) and (8). Entries marked with an asterisk (*) were inferred using a Gegenbauer polynomial expansion, following the corresponding reference. In those with (†), we use the simple polynomial form described in Ref. [30]. Uncertainties have been symmetrized. Here, $\bar{x} = 1 - x$.

	$\langle\xi\rangle_{\zeta_2}^K$	$\langle\xi^2\rangle_{\zeta_2}^K$	$\langle 1/x\rangle_{\zeta_2}^K$	$\langle 1/\bar{x}\rangle_{\zeta_2}^K$
This work	0.082(7)	0.239(9)	4.03(18)	2.89(11)
lQCD 22' [13]	0.065(31)*	0.258(32)	4.18(23)*	3.28(23)*
lQCD 20' [30]	0.002(69)†	0.198(16)	2.97(42)†	2.94(42)†
lQCD 19' [31]	0.032(12)	0.231(4)	3.43(8)*	3.28(23)*
QCD SR [39]	0.024(12)*	0.261(36)*	3.66(32)*	3.42(32)*
CSM DB [24]	0.035(5)	0.24(1)	3.271	3.21
CSM RL [38]	0.11	0.23	4.20	2.72

The inverse moments of the DA provide another measure of its asymmetry. Here, we find ($\bar{x} = 1 - x$),

$$\langle 1/x\rangle_{\zeta_2}^K = 4.03(18), \qquad \langle 1/\bar{x}\rangle_{\zeta_2}^K = 2.89(11). \tag{12}$$

As revealed in Table I, distributions with more asymmetric profiles (hence, larger $\langle\xi\rangle_{\zeta_2}^K$ moments) lead to a greater difference between the inverse moments. Thus, these values also encode the degree of $SU_F(3)$ FSB. In this sense, and due to their relationship with HSFs, large virtuality EMFFs are extremely useful in their determination.

IV. KAON ELECTROMAGNETIC FORM FACTORS

Following the procedure outlined in the previous section, the result of our LO exploration of the ratio of neutral-to-charged kaon EMFFs is presented in Fig. 2. The agreement with the experimental data from Ref. [1] is evident, to the extent that the fit provided by the BESIII collaboration for this ratio, 0.21 ± 0.01, falls entirely within our set of replicas. In the same figure, we also depict the outcome arising from the lQCD kaon DA—determined in Ref. [13] and depicted herein in Fig. 1. The resulting $\mathcal{R}_K$ would also remain within our estimates. For further comparison, Fig. 2 includes the RL and DB kernel LO expectations for $\mathcal{R}_K$. The former produces the more asymmetric kaon DA among all cases (see Fig. 1), leading to a stronger $SU_F(3)$ FSB and, consequently, a larger neutral-to-charged kaon EMFF ratio. In contrast, the DB kernel, which features a broad and slightly asymmetric kaon DA, generates a $\mathcal{R}_K$ with a magnitude that is three times smaller. Both cases, RL and DB, are outside our acceptable region and, to some extent, could be interpreted as boundaries.

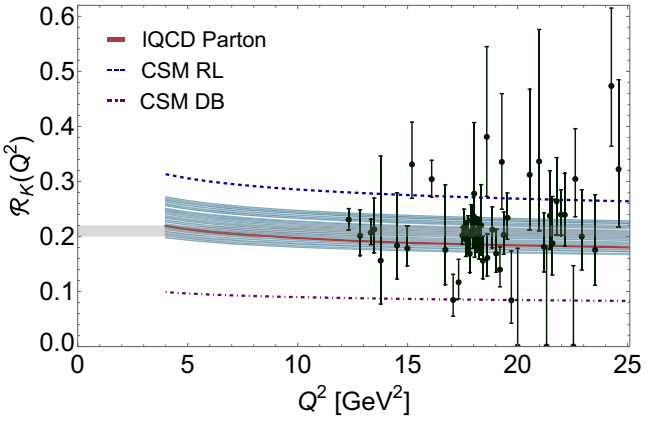

FIG. 2. Ratio of neutral-to-charged kaon EMFFs, $\mathcal{R}_K$, obtained at LO according to the formulae in Eqs. (1)–(3) and the DAs discussed in the text. Labels and references are the same as in Fig. 1. The experimental data points are those determined by the BESIII collaboration, with the gray rectangle representing the best fit reported therein, i.e., 0.21 ± 0.01 [1].

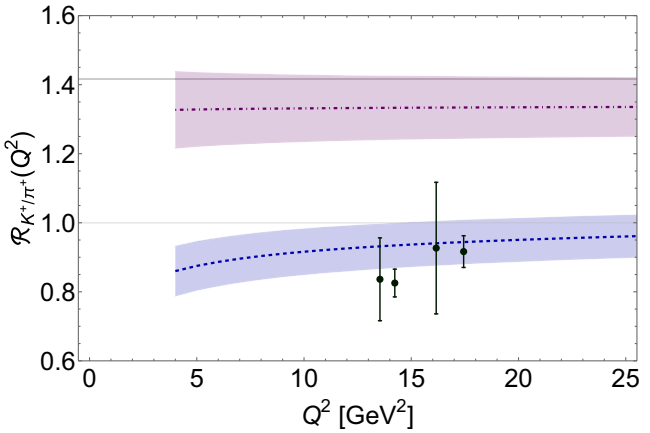

FIG. 3. Ratio of charged kaon-to-pion EMFFs, $\mathcal{R}_{K^+/\pi^+}$, obtained through the LO HSF, Eqs. (1)–(3). For $F_{K^+}(Q^2)$, we adopt the mean of the replica set along with a 1-σ error band. For the construction of $F_{\pi^+}(Q^2)$, two DAs are considered: one corresponding to $\langle\xi^2\rangle^\pi_{\zeta_2} = 0.24$ (purple, dot dashed), and another to $\langle\xi^2\rangle^\pi_{\zeta_2} = 0.28$ (blue, dashed). Experimental (timelike) data taken from Ref. [46]. The upper grid line indicates the asymptotic limit, $f_K^2/f_\pi^2 \approx 1.43$.

As evidenced by this analysis, employing a LO prescription requires producing a kaon DA with greater splitting between its inverse moments, $\langle 1/x, 1/\bar{x}\rangle^K_{\zeta_2}$. Only in this way can the correct magnitude for $\mathcal{R}_K$ be obtained. In other words, to be consistent with the available experimental data—which lies within the $12 < Q^2 < 25$ GeV^2 range—a LO treatment results in a larger skewness for $\varphi_K^l(x;\zeta_2)$. Given that higher-order corrections to the HSF tend to increase $\mathcal{R}_K$ [14], we expect that incorporating these contributions within our data-driven approach will yield a more symmetric kaon DA. Consequently, the effects of explicit $SU_F(3)$ FSB in shaping the kaon wavefunction would be attenuated, making QCD's mass generation even more dominant. A similar outcome is observed for the kaon distribution function [45].

A final piece for examination is the charged kaon-to-pion EMFFs ratio,

$$\mathcal{R}_{K^+/\pi^+}(Q^2) := F_{K^+}(Q^2)/F_{\pi^+}(Q^2). \tag{13}$$

The derivation of the charged kaon EMFF, $F_{K^+}(Q^2)$, follows straightforwardly from our obtained set of replicas and Eq. (1). For the pion, we employ the LO HSF together with the parametric representation of Eq. (5) for the corresponding DA. We consider two limiting cases, namely, $\langle\xi^2\rangle^\pi_{\zeta_2} = 0.24,\ 0.28$. The first value lies within the range of the lQCD results reported in Refs. [30,31], as well as the CSM prediction with the DB kernel [23,24]. The second case yields a broader pion DA and aligns more closely with the RL truncation result [23] and the lQCD expectation from [13].

The derived result is displayed in Fig. 3. The pion characterized by $\langle\xi^2\rangle^\pi_{\zeta_2} = 0.24$ features an inverse moment $\langle 1/x\rangle^\pi_{\zeta_2} = 3.46$. Thus, with our kaon values listed in Table I, the LO HSF rapidly approaches the asymptotic limit f_K^2/f_π^2. In contrast, for a broader pion DA, corresponding to $\langle\xi^2\rangle^\pi_{\zeta_2} = 0.28$ and $\langle 1/x\rangle^\pi_{\zeta_2} = 4.39$, such a limit would be reached at a much slower rate. In this case, the LO HSF leads to $\mathcal{R}_{K^+/\pi^+} \lesssim 1$ over a wide range of photon virtualities. This profile is more consistent with the timelike experimental data [46]. Nonetheless, since $F_{\mathbf{P}}(0) = 1$ is fixed by charge conservation, and the kaon charge radius (a measure of the slope near $Q^2 \approx 0$) is smaller than that of the pion [47,48], the above implies that $F_{\pi^+}(Q^2)$ would intersect $F_{K^+}(Q^2)$ at some point. It is not clear why this would happen. What is clear is that, by restricting ourselves to a LO analysis, a larger magnitude of $F_{\pi^+}(Q^2)$ is required in order to bring the ratio $\mathcal{R}_{K^+/\pi^+}$ closer to the experimental data. This is achieved with a broader pion DA, as such a distribution exhibits a steeper fall-off at the endpoints. In any case, it is important to note that while the dynamics around $Q^2 \approx 0$ is governed by vector meson dominance [49,50], and the asymptotic behavior by Eq. (1), there is no established prescription for intermediate spacelike values of photon virtualities.

V. SUMMARY AND SCOPE

We have introduced a data-driven approach to determine the kaon DA at an experimentally accessible scale of $\zeta = 2$ GeV, $\varphi_K^l(x;\zeta_2)$. The procedure described here relies on a simple yet effective two-parameter model for the kaon DA that properly captures the broadening and skewness effects induced by the mechanisms of DCSB and $SU_F(3)$ FSB. The model parameters are determined from recent

empirical information on the neutral-to-charged kaon EMFF ratio $\mathcal{R}_K$. For this purpose, the HSFs in QCD are employed at the LO level of approximation. The required DAs are fixed in such a way that the model parameters are randomly scanned within a sensible range, informed by lQCD and continuum methods. Our analysis highlights the necessity of employing representations for $\varphi_K^l(x;\zeta_2)$ that properly reproduce the DA's dilation and skewness while adhering to the soft endpoint behavior prescribed by QCD. These points are vital in ensuring the correct magnitude for $\mathcal{R}_K$. Moreover, the kaon DAs obtained through our procedure capture the effects of DCSB by yielding broadened profiles. Conversely, the distributions also exhibit a rather visible asymmetry. To a large extent, this stems from the fact that at this level of approximation (LO, leading-twist), a larger splitting between the inverse moments $\langle 1/x, 1/(1-x)\rangle$ is produced. It is expected that the enhancement of the value of $\mathcal{R}_K$ due to higher-order corrections will soften this asymmetry. Despite these facts, our analysis captures well-established patterns from both continuum and lattice QCD methods. Among other implications, it is seen that the distortion of the kaon wavefunction is not so marked. Consequently, the present evaluation, which should be interpreted as a limiting case, reveals that the explicit breaking of the $SU_F(3)$ flavor symmetry is subdominant compared to the nonperturbative effects of QCD. In this regard, the incorporation of higher-order effects in the hard-scattering kernels is expected to further reduce the skewness. This shall be addressed elsewhere. On the other hand, the examination of the charged kaon-to-pion EMFF ratio shows that, despite meeting the asymptotic expectations, this value could lie below unity given a sufficiently dilated pion DA. Nonetheless, it is likely that the present level of approximation is responsible for the broader pion DA and that the inclusion of higher-order effects will yield a more realistic distribution. A precise determination of its profile is therefore crucial. Finally, it is anticipated that with future experimental efforts on the pion and kaon EMFFs, the present data-driven approach may prove instrumental in yielding a precise determination of the corresponding wavefunctions.

ACKNOWLEDGMENTS

This work is supported by the National Natural Science Foundation of China (Grants No. 12135007 and No. 11875169); the Spanish Ministry of Science and Innovation (MICINN, Grant No. PID2022-140440NB-C22); and Junta de Andalucía (Grant No. P18-FR-5057).

DATA AVAILABILITY

The data that support the findings of this article are openly available [1].

[1] M. Ablikim *et al.* (BESIII Collaboration), Phys. Rev. Lett. **132**, 131901 (2024).
[2] K. K. Seth, S. Dobbs, A. Tomaradze, T. Xiao, and G. Bonvicini, Phys. Lett. B **730**, 332 (2014).
[3] G. R. Farrar and D. R. Jackson, Phys. Rev. Lett. **43**, 246 (1979).
[4] G. P. Lepage and S. J. Brodsky, Phys. Lett. **87B**, 359 (1979).
[5] G. P. Lepage and S. J. Brodsky, Phys. Rev. D **22**, 2157 (1980).
[6] A. V. Efremov and A. V. Radyushkin, Phys. Lett. **94B**, 245 (1980).
[7] F. Gao, L. Chang, Y.-X. Liu, C. D. Roberts, and P. C. Tandy, Phys. Rev. D **96**, 034024 (2017).
[8] L.-B. Chen, W. Chen, F. Feng, and Y. Jia, Phys. Rev. Lett. **132**, 201901 (2024).
[9] R. D. Field, R. Gupta, S. Otto, and L. Chang, Nucl. Phys. **B186**, 429 (1981).
[10] F. M. Dittes and A. V. Radyushkin, Sov. J. Nucl. Phys. **34**, 293 (1981).
[11] M. H. Sarmadi, Phys. Lett. **143B**, 471 (1984).
[12] E. Braaten and S.-M. Tse, Phys. Rev. D **35**, 2255 (1987).
[13] J. Hua *et al.* (Lattice Parton Collaboration), Phys. Rev. Lett. **129**, 132001 (2022).
[14] L.-B. Chen, W. Chen, F. Feng, and Y. Jia, Phys. Lett. B **870**, 139886 (2025).
[15] J. Bijnens and A. Khodjamirian, Eur. Phys. J. C **26**, 67 (2002).
[16] J. Chai and S. Cheng, J. High Energy Phys. 06 (2025) 229.
[17] H.-T. Ding, X. Gao, A. D. Hanlon, S. Mukherjee, P. Petreczky, Q. Shi, S. Syritsyn, R. Zhang, and Y. Zhao, Phys. Rev. Lett. **133**, 181902 (2024).
[18] A. Accardi *et al.*, Eur. Phys. J. A **52**, 268 (2016).
[19] A. Accardi *et al.*, Eur. Phys. J. A **60**, 173 (2024).
[20] C. D. Roberts, D. G. Richards, T. Horn, and L. Chang, Prog. Part. Nucl. Phys. **120**, 103883 (2021).
[21] M. Ding, C. D. Roberts, and S. M. Schmidt, Particles **6**, 57 (2023).
[22] K. Raya, A. Bashir, D. Binosi, C. D. Roberts, and J. Rodríguez-Quintero, Few-Body Syst. **65**, 60 (2024).
[23] L. Chang, I. C. Cloet, J. J. Cobos-Martinez, C. D. Roberts, S. M. Schmidt, and P. C. Tandy, Phys. Rev. Lett. **110**, 132001 (2013).

[24] Z.-F. Cui, M. Ding, F. Gao, K. Raya, D. Binosi, L. Chang, C. D. Roberts, J. Rodríguez-Quintero, and S. M. Schmidt, Eur. Phys. J. C **80**, 1064 (2020).
[25] S. V. Mikhailov, A. V. Pimikov, and N. G. Stefanis, Phys. Rev. D **93**, 114018 (2016).
[26] N. G. Stefanis, Phys. Rev. D **102**, 034022 (2020).
[27] S. Cheng, A. Khodjamirian, and A. V. Rusov, Phys. Rev. D **102**, 074022 (2020).
[28] Q. Chang, S. J. Brodsky, and X.-Q. Li, Phys. Rev. D **95**, 094025 (2017).
[29] R. Swarnkar and D. Chakrabarti, Phys. Rev. D **92**, 074023 (2015).
[30] R. Zhang, C. Honkala, H.-W. Lin, and J.-W. Chen, Phys. Rev. D **102**, 094519 (2020).
[31] G. S. Bali, V. M. Braun, S. Bürger, M. Göckeler, M. Gruber, F. Hutzler, P. Korcyl, A. Schäfer, A. Sternbeck, and P. Wein (RQCD Collaboration), J. High Energy Phys. 08 (2019) 065; 11 (2020) 37.
[32] S. S. Agaev, V. M. Braun, N. Offen, and F. A. Porkert, Phys. Rev. D **83**, 054020 (2011).
[33] B. Blossier, M. Mangin-Brinet, J. M. Morgado Chávez, and T. San José, J. High Energy Phys. 09 (2024) 079.
[34] M. Ding, F. Gao, L. Chang, Y.-X. Liu, and C. D. Roberts, Phys. Lett. B **753**, 330 (2016).
[35] F. E. Serna, R. C. da Silveira, J. J. Cobos-Martínez, B. El-Bennich, and E. Rojas, Eur. Phys. J. C **80**, 955 (2020).
[36] Y.-Z. Xu, Phys. Rev. D **111**, 114012 (2025).
[37] V. L. Chernyak and A. R. Zhitnitsky, Phys. Rep. **112**, 173 (1984).
[38] C. Shi, L. Chang, C. D. Roberts, S. M. Schmidt, P. C. Tandy, and H.-S. Zong, Phys. Lett. B **738**, 512 (2014).
[39] A. Khodjamirian, T. Mannel, and M. Melcher, Phys. Rev. D **70**, 094002 (2004).
[40] S. S. Agaev, V. M. Braun, N. Offen, and F. A. Porkert, Phys. Rev. D **86**, 077504 (2012).
[41] V. M. Braun, A. Khodjamirian, and M. Maul, Phys. Rev. D **61**, 073004 (2000).
[42] Z.-Q. Yao, D. Binosi, and C. D. Roberts, Phys. Lett. B **855**, 138823 (2024).
[43] G. P. Lepage and S. J. Brodsky, Phys. Rev. D **22**, 2157 (1980).
[44] Y. Lu, Y.-Z. Xu, K. Raya, C. D. Roberts, and J. Rodríguez-Quintero, Phys. Lett. B **850**, 138534 (2024).
[45] Z.-N. Xu, D. Binosi, C. Chen, K. Raya, C. D. Roberts, and J. Rodríguez-Quintero, Phys. Lett. B **865**, 139451 (2025).
[46] K. K. Seth, S. Dobbs, Z. Metreveli, A. Tomaradze, T. Xiao, and G. Bonvicini, Phys. Rev. Lett. **110**, 022002 (2013).
[47] Z.-F. Cui, D. Binosi, C. D. Roberts, and S. M. Schmidt, Chin. Phys. C **46**, 122001 (2022).
[48] S. Navas *et al.* (Particle Data Group), Phys. Rev. D **110**, 030001 (2024).
[49] H. B. O'Connell, B. C. Pearce, A. W. Thomas, and A. G. Williams, Prog. Part. Nucl. Phys. **39**, 201 (1997).
[50] G. J. Gounaris and J. J. Sakurai, Phys. Rev. Lett. **21**, 244 (1968).